Mechanism of Crystallization and Implications for Charge Transport in Poly(3-ethylhexylthiophene) Thin Films

*Duc T. Duong, Victor Ho, Zhengrong Shang, Sonya Mollinger, Stefan C.B. Mannsfeld, Javier Dacuña, Michael F. Toney, Rachel Segalman, and Alberto Salleo**

In this work, crystallization kinetics and aggregate growth of poly(3-ethylhexylthiophene) (P3EHT) thin films are studied as a function of film thickness. X-ray diffraction and optical absorption show that individual aggregates and crystallites grow anisotropically and mostly along only two packing directions: the alkyl stacking and the polymer chain backbone direction. Further, it is also determined that crystallization kinetics is limited by the reorganization of polymer chains and depends strongly on the film thickness and average molecular weight. Time-dependent, field-effect hole mobilities in thin films reveal a percolation threshold for both low and high molecular weight P3EHT. Structural analysis reveals that charge percolation requires bridged aggregates separated by a distance of ≈2–3 nm, which is on the order of the polymer persistence length. These results thus highlight the importance of tie molecules and inter-aggregate distance in supporting charge percolation in semiconducting polymer thin films. The study as a whole also demonstrates that P3EHT is an ideal model system for polythiophenes and should prove to be useful for future investigations into crystallization kinetics.

1. Introduction

Semiconducting polymers have garnered considerable interests over recent years due to their solution processability, increasingly high performance, and potential use in numerous applications ranging from flexible light-emitting diodes to photovoltaics.[1–3] The latitude in creating new materials from organic synthesis combined with long standing knowledge of thin film polymer processing have allowed researchers to achieve field-effect mobilities and solar cell efficiencies exceeding conventional amorphous silicon technologies.[4–6] Yet, despite drastic improvements on the materials front, it remains a challenge to understand the mechanism of film growth and crystallization and how such processes can lead to efficient electronic charge transport in these systems. In stark contrast to traditional semiconductor technologies where single crystal semiconductors (Si, Ge, GaAs, etc.) can be grown from the melt with exquisite control over defect concentrations, crystallization in polymer thin films is vastly more convoluted and both computationally and empirically difficult to describe. The coexistence of both disordered and ordered domains, the anisotropic shape of the individual crystallites and the generally weak nature of both interchain and intrachain van der Waals interactions all contribute to the complexity of the crystallization process.[7,8] The description of the microstructure of a pure, semiconducting polymer film, for instance, involves multiple length scales as a consequence of the different types of intermolecular forces.[9] Further, the microstructure of polymer thin films deposited by spin casting (1–10 s) and by recrystallizing from the melt at room temperature (< 1 s) develops on too short of a time scale for most detailed kinetic studies.[10] In a recent study, Vakhshouri et al. were able to monitor recrystallization for P3HT at higher quenching temperatures.[11] Chou et al. has also managed to reveal some of the intricacies in spin casting polymer-fullerene blends.[12] In both cases, however, no experimental details regarding the growth of individual aggregates and crystallites or the distribution of such ordered domains within the amorphous matrix are presented.

Within the current body of literature, the crystallization mechanism is not known for any semiconducting polymer. The growth rate of crystallites and aggregates along the three different molecular packing directions, for instance, cannot be measured for most systems due to limitations presented above. We thus turn our attention to what we consider to be an ideal model system: the polymer poly(3-ethylhexylthiophene)

D. T. Duong, Z. Shang, S. Mollinger, Prof. A. Salleo
Department of Materials Science and Engineering
Stanford University
Stanford, California 94305, USA
E-mail: asalleo@stanford.edu
V. Ho, Prof. R. Segalman
Department of Chemical and Biomolecular Engineering
University of California, Berkeley
Materials Science Division
Lawrence Berkeley National Laboratory
Berkeley, California 94720, USA
Dr. S. C. B. Mannsfeld, Dr. M. F. Toney
Stanford Synchrotron Radiation Lightsource
SLAC National Accelerator Laboratory
Menlo Park, California 94025, USA
J. Dacuña
Department of Electrical Engineering Stanford University
Stanford, California 94305, USA

DOI: 10.1002/adfm.201304247

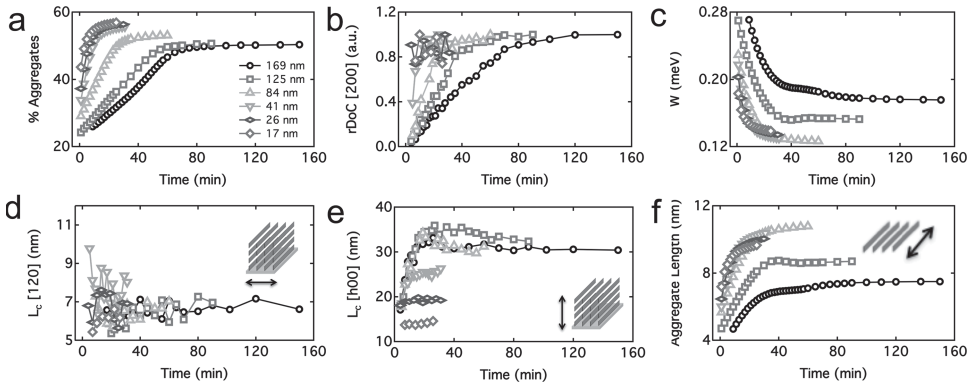

Figure 1. Summary of time-dependent a) percent aggregates, b) rDoC, c) excitonic bandwidths, d) coherence lengths along the π-stacking direction, e) crystallite size along the alkyl stacking direction, and f) aggregate lengths along the chain backbone. Percent aggregates, excitonic bandwidths, and aggregate lengths are extracted from models by Spano and Giershner[18,23] while rDoC values are calculated from pole figures. Coherence lengths along the (120) and crystallite sizes along the (h00) directions are determined using Scherrer's equation and Williamson Hall analysis, respectively.

(P3EHT) first reported by Ho et al.[13] A relative of the ubiquitous poly(3-hexylthiophene) (P3HT), P3EHT exhibits similar optoelectronic properties and the same semicrystalline solid-state morphologies in thin film: ordered domains coexisting with amorphous, disordered regions. Such similarity allows us to study P3EHT thin films using the powerful models and characterization techniques that have been developed for P3HT over the last few decades. The aspect of P3EHT that we want to exploit here, however, is its slow recrystallization kinetics. As was previously shown, thin films of P3EHT may take up to several hours to recrystallize at room temperature after being quenched from a melt.[10] This property allows us to carefully observe the crystallization of the polymer film using quantitative analyses of grazing incidence X-ray diffraction (GIXD) and optical absorption spectroscopy. We can then correlate the evolution of such microstructures to the evolution of electronic properties in devices. Such a study allows us to identify both the mechanism of crystallization and the microstructures responsible for efficient charge transport in semiconducting polymers.

In this study we investigate the mechanism of crystallization in spin cast, melt-recrystallized P3EHT thin films of different thicknesses. Time-dependent structural and optical measurements reveal that P3EHT aggregates grow anisotropically and in a nearly one-dimensional manner along the polymer chain backbone. Furthermore, we show that crystallization kinetics is faster in thinner films and for lower molecular weight polymers due to chain confinement effects. Time-dependent electrical measurements on field-effect transistors also reveal a percolation onset for charge transport in both low and high molecular weight polymers. We attribute this onset to the formation of ordered aggregates connected by bridging tie chains. Although previous works have shown the existence of tie chains,[14,15] it is not known how charges move through them and whether or not the length of tie chains within amorphous domains play an important role for charge transport. Here we show that tie chains allow for percolation even in short chain (<10 kDa) polymers and are only effective at bridging aggregates spaced within a relatively short distance from each other.

2. Results and Discussion

2.1. Crystallization Mechanism of Individual Aggregates/Crystallites

We first address the molecular packing of P3EHT in the solid state. Boudouris et al. showed that P3EHT exhibits a substantially different unit cell than that of P3HT.[10] However, refined crystal structure calculations of GIXD data using previously established methods[16] (data not shown) reveal that P3EHT does pack with the same anisotropic structural motif as P3HT: π- and alkyl stacked polymer chains oriented edge-on (≈100%) with respect to the substrate. Determining the exact crystal structure is outside the scope of this report and will be the subject of a separate publication. Nevertheless, due to structural similarities between the two polymers, we are able to apply to P3EHT thin films numerous models and characterization techniques developed specifically for P3HT. For instance, the optical absorption and emission spectra of P3EHT display the same features as those of P3HT. We will also use the same distinction between different structural species previously presented, wherein an aggregate composes of π-stacked polymer chains and a crystallite consists of alkyl-stacked aggregates.[17]

Spin cast P3EHT thin films of different thicknesses (M_w = 6.9 kDa, M_n = 6.5 kDa, PDI = 1.06) are melted at 120 °C, quenched to room temperature, and then monitored over time using a combination of 2D GIXD and optical absorption. Time-dependent absorption spectra of P3EHT are fitted using a weakly coupled H-aggregate model by F.C. Spano, which allows for the determination of the percent aggregates.[18–20] Pole figures are also compiled from the GIXD patterns and the relative degrees of crystallinity (rDoC) are calculated according to our previous report.[10] These quantitative analyses show that, after quenching, both the percent aggregates and the rDoC's increase as the films recrystallize (**Figure 1**a,b). In addition, the kinetics of this process is thickness-dependent. A 17 nm film, for instance, stabilizes within ≈30 min whereas a 169 nm film takes up to 80–90 min to fully recrystallize. This thickness dependence can be attributed either to preferential heterogeneous film growth from the substrate-polymer and air-polymer

interfaces, or to reduced degrees of freedom of the chains due to confinement effects forcing the molecules in configurations favorable to crystallite growth. We will show that the latter is the main mechanism for enhanced crystallization kinetics in thinner films.

A more sophisticated analysis of optical absorption and X-ray diffraction is also used to monitor the kinetics and shape evolution of individual aggregates and crystallites. According to a model by Gierschner et al., interaction lengths of a polymer chain within an aggregate can be calculated from the excitonic bandwidths (W), which are extracted from a Spano fit to the absorption spectra[18,19] (see supporting information). Further, we estimate the crystallite size along the alkyl stacking direction and the coherence length along the π-stacking directions by analyzing (h00) and (120) peak widths, respectively. Note that the (120) crystallographic direction is not exactly along the π-stacking direction though the difference between the two is within only a few degrees.[21] Such a combination of techniques allows us to calculate the average coherence lengths along all three molecular packing directions as a function of time. The results show, firstly, that the coherence length along the (120) planes does not change significantly over the time span of the recrystallization process (Figure 1d) and remains around ≈6–9 nm as calculated from Scherrer's equation. This suggests that aggregates nucleate and grow very quickly along the π-stacking direction (<1 min), and do not refine their structure along this direction at longer times as the films recrystallize. Note that additional growth may exist along the π-stacks at long times. However, chains separated by a distance longer than the estimated 6–9 nm are not coherent and thus considered to be different entities. For instance, "π-stacks" with a size of 12–18 nm would be structurally defined as two separate, aggregated species.

In contrast, crystallites do grow along the alkyl stacking (h00) direction (Figure 1e) from an initial size of ≈12 nm to a characteristic size of ≈30–32 nm at an estimated rate of 1.4 nm per minute, as calculated from a Williamson Hall analysis. The size of crystallites in films close to or thinner than 30–32 nm is confined to that of the film thickness, similar to that observed for P3HT.[22] In other words, a 17 nm film would only contain crystallites equal to or smaller than 17 nm in size along the alkyl direction. Interestingly the growth rate along (h00) is thickness independent for films above the characteristic crystallite size. This suggests that crystallites are not growing in a bottom-up fashion from the interfaces but are instead nucleating throughout the thickness of the film. To evaluate this hypothesis, we investigate the effect of surface treatment on recrystallization dynamics in thin films. As shown in **Figure 2**a the type of self-assembled monolayers do not significantly affect the kinetics of film growth. We do notice that films spin cast on OTS (octadecyltrichlorosilane) dewet upon melting and may explain the slightly slower recrystallization kinetics observed. Nevertheless, the choice of interface does not significantly impact the crystallization kinetics. In other words, though the microstructure at the interface may be very different from that in the bulk, preferential nucleation and growth from the interfaces does not dominate the recrystallization process.

Finally, we note that although growth along the alkyl and π-stacking directions stops after ≈20 min for thicker films,

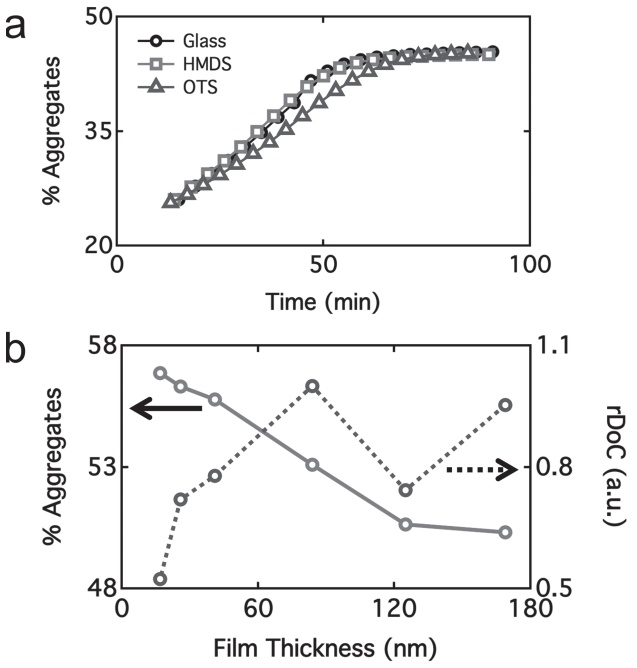

Figure 2. a) Percent aggregates as a function of time for spin-cast 181 nm thick films on different surfaces. As shown, surface energies seem to not significantly affect the recrystallization kinetics. Also plotted are b) percent aggregates and ~rDoC as a function of film thickness.

crystallization continues for much longer. Indeed after 20 min, a 169 nm film is only ≈30% as crystalline and ≈60% as aggregated as its final state. We show here that the remaining crystallization is attributed to growth of aggregates and crystallites along the polymer chain backbone. Figure 1f shows that the time scale over which aggregate length growths, as calculated from W (Figure 1c),[23] matches that of film recrystallization (Figure 1a and Supporting Information, Figure S6). This type of growth most likely results from chain reorganization and is shown to occur faster as the film thickness decreases. For all films, aggregates grow from initial lengths of ≈3–6 nm to final lengths of ≈7–11 nm. Thus the mechanism of recrystallization at long times is dominated by aggregate and crystallite growth along the chain backbone direction, as depicted in **Figure 3**.

Here we would like to address the difference between aggregates and crystallites in the context of growth and crystallization. As we have described in a previous publication,[17] the "degree of aggregation" is related to the density of π-stacked polymer chains while "crystallinity" refers to the volume frac-

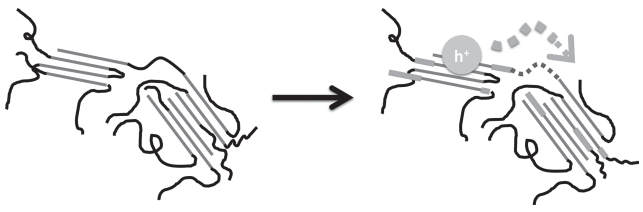

Figure 3. A schematic demonstrating how the reorganization of polymer chains leads to chain extension (bold segments) and thereby aggregate growth. Charge percolation is expected to occur once the bridging tie chain (dotted) is on the order of the polymer persistence length.

Table 1. Summary of extracted parameters from the Avrami fit for P3EHT films of different thicknesses.

Film Thickness [nm]	*k*	*n*
169	0.000122	2.34
125	0.00328	1.61
84	0.0111	1.59
41	0.0826	1.26
26	0.184	1.04
17	0.239	1

tion of the film which is alkyl stacked. This was demonstrated by comparing the percent aggregates and relative degree of crystallinity (rDoC) as a function of film thickness.[17,22] The results showed that thinner films are generally more aggregated and less crystalline as is defined above. In Figure 2b we plot the percent aggregates and ~rDoC as a function of film thickness for low MW P3EHT. Clearly the same trend is observed for P3EHT and supports the idea that, similar to P3HT, P3EHT aggregates and crystallites are distinct. Based upon these definitions, crystallites have three different available growth directions while aggregates have only two: the π-stacking and polymer chain backbone directions. It is therefore important to keep this distinction in mind when comparing crystallization rates from different techniques. Diffraction and calorimetry, for instance, generally probe crystallites while optical measurements tend to probe aggregates.

Since aggregates are shown above to grow along only one direction, in this case the chain backbone, they exhibit one-dimensional growth kinetics. To this end we fit the time-dependent percent aggregates for all film thicknesses using a modified Avrami model:

$$A = A_g(1 - \exp(kt^n)) + A_o \quad (1)$$

Here A is the total percent aggregates, A_o is the initial percent aggregates ($t = 0$), A_g is the percent aggregates gained at long times (the sum of A_o and A_g is the final percent aggregates of the film), and k and n are Avrami parameters related to the growth kinetics. We are interested in n, the dimensionality of the recrystallization process. For nearly all P3EHT thin films n lies roughly between 1 and 2 (**Table 1**), which is in agreement with the hypothesized one-dimensional growth.[24] Thus the rate-limiting step for thin film recrystallization lies in the reorganization and extension of polymer chains that lead to aggregate growth along chain backbones. This conclusion is consistent with the faster growth rate along the chain backbone (Figure 1f) and the higher degree of aggregation in thinner films (Figure S5, Supporting Information). It also provides an explanation for the thickness dependent crystallization kinetics. In thicker films, polymer chains have a higher degree of freedom and can be oriented perpendicular or parallel to the substrate.[25] However, as the film thickness decreases, chain backbones are forced to lie more parallel to the substrate and thus less likely to become entangled with adjacent chains. This supposition is supported by an observed decrease in the FWHM of the pole figures (see supporting information), which implies that thinner films are better oriented than thicker films. We hypothesize that this suppression of polymer chains' degrees of freedom through thickness confinement improves the ease of chain reorganization, resulting in enhanced crystallization kinetics in thinner films of P3EHT.

To ensure that these growth mechanisms do not apply only to low molecular weight polymers, we also perform detailed structural studies on a higher molecular weight batch of P3EHT (M_n = 22 kDa). The results show that, in higher molecular weight P3EHT, aggregates also form in one dimension and the crystallization kinetics are thickness-dependent. The main effect of the increased molecular weight is on the rate of recrystallization, which occurs ≈1.5–2 times more slowly than that of the lower molecular weight polymer (see supporting information). This difference is attributed to more twists and bends that exist in longer polymer chains and, as a result, a higher energy barrier for chain reorganization. Hence the observed mechanism for crystallite growth is general for P3EHT and may describe crystallization in other polythiophenes as well. Isothermal crystallization of bulk P3ATs, for instance, was shown by differential scanning calorimetry (DSC) to yield n values well below 2.[26–28] P3HT crystallization within bulk heterojunctions also exhibit a diffusion-controlled growth process with n values ≈1.[29] These slower growth kinetics were explained by the slow diffusion rate of individual polymer chains, which is in good agreement with our results.

2.2. Relating Thin Film Microstructure to Charge Percolation

The slow growth of aggregates and crystallites can be exploited to understand charge transport and percolation in P3EHT thin films. Towards this end we fabricate bottom-gate, bottom-contact FETs by spin casting P3EHT onto gold-patterned Si substrates with a 200 nm thermal oxide layer. In melt-annealed films quenched at room temperature, the mobility increases over time from ≈10^{-6} to ≈5×10^{-5} cm^2 V^{-1} s^{-1}, consistent with previous findings,[10] and occurs more quickly for thinner films and lower molecular weights (**Figure 4**). Interestingly the increase in field-effect mobility as a function of time is thickness-dependent even though transport in FETs occurs only within the first 1–2 polymer layers.[30] We thus conclude that the transport layer, represented by the polymer-dielectric interface, grows at nearly the same rate as the bulk film. This observation further supports our proposed model where aggregates do not grow preferentially from the interface(s) but instead throughout the thickness of the film.

We also collect absorption spectra of films spin cast from the same solution onto glass substrates and obtain time-dependent percent aggregates for each thicknesses. Below we plot the field-effect hole mobility as a function of percent aggregates for two films of low and high molecular weights (Figure 4c). Because FETs only probe transport within the first few nanometers of the film, we focus here only on thin films such that the structure of the entire film reflects that of the interface (see supporting information for complete data sets).[17] Surprisingly we observe a clear percolation onset in charge transport even for low molecular weight P3EHT: above a certain threshold, the mobility increases exponentially as a function of percent

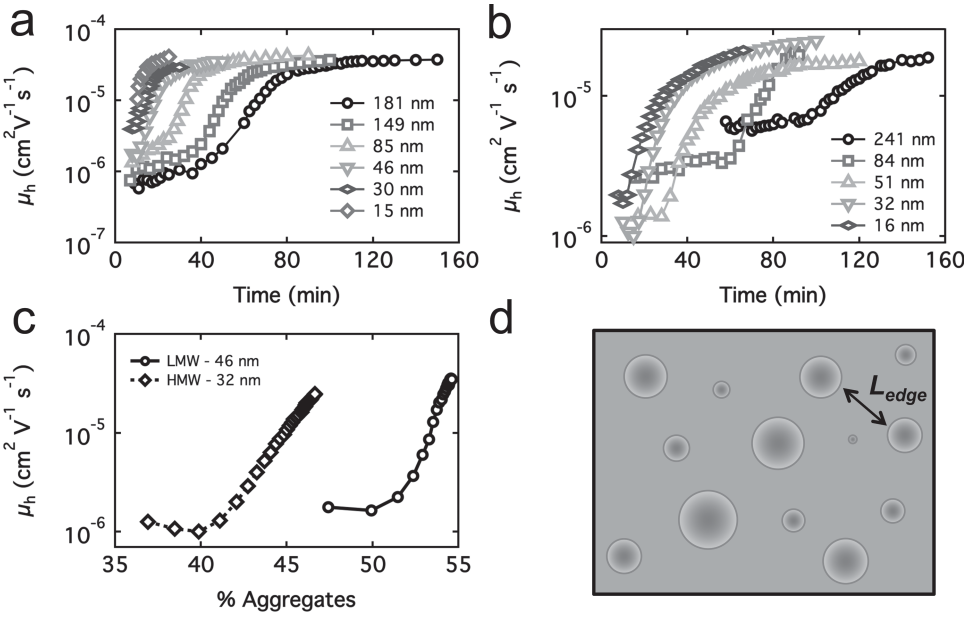

Figure 4. Plot of field-effect hole mobilities as a function of time in films of different thicknesses for a) lower molecular weight and b) high molecular weight P3EHT. c) Plot of the field-effect hole mobilities as a function of percent aggregates in thin films of LMW and HMW P3EHT. A clear percolation onset is observed in both cases. d) Top down view of a P3EHT thin film wherein 2-dimensional, circular aggregates nucleate and grow from a melted, amorphous matrix.

aggregates. The lower observed onset for higher molecular weight P3EHT suggests that charge transport can occur more efficiently at lower aggregate densities when longer chains are present.

In order to explain these phenomena, we first consider requirements for charge percolation in semiconducting polymer thin films. Previous studies have shown evidence to suggest that interconnecting polymer aggregates are required for efficient charge transport. According to these models, charges can percolate when a single chain is able to bridge two otherwise isolated aggregates. Such a model explains the drastic increase in field-effect mobility as molecular weight increases.[31–33] A P3EHT polymer chain with an M_n of 6.5 kDa, however, is only ≈13 nm long whereas its average aggregate length is ≈7–11 nm (Figure 1d). It is therefore too short to fully span two isolated aggregates (in most physical circumstances) and should not exhibit a percolation onset in field-effect mobility. Thus we hypothesize that effective charge percolation in semiconducting polymer thin films can be achieved through relatively short (≈2–3 nm) connecting tie chains. In such cases, polymer chains can bridge two aggregates given that i) at least parts of the chain reside in each aggregate and ii) the portion of the chain that resides in the amorphous region must be on the order of the polymer's persistence length. For P3EHT, the solution persistence length has been estimated to be ≈3.0 nm, which is close to values of ≈2.4–2.9 nm determined for P3HT.[34–36]

To evaluate this hypothesis we first calculate the average size of an aggregate and the average distance between aggregates at the percolation onset based on the structural and optical data presented previously. The percolation thresholds in thinner films are estimated to be ≈50–54% and ≈40–42% for low (LMW) and high (HMW) molecular weight P3EHT, respectively, at which point the average aggregate size from a top-down view of the film is ≈10 × 7 nm (LMW) and ≈7 × 6 nm (HMW). To make the problem tractable, we approximate the aggregates as circles with the same area as the average aggregate area derived from our experimental data (Figure 2d). Since the aspect ratios of growing aggregates only range between ~1-1.5 (see supporting information), we believe this approximation to be valid. The corresponding diameters (d_{agg}) are ≈9.4 nm (LMW) and ≈7.3 nm (HMW). By dividing the fraction aggregates (*FA*) by the total area of a single aggregate (A_{agg}), we can obtain the number aggregate densities at percolation. Furthermore, we determine the average distance between the centers of individual aggregates (L_{agg}) according to Equation (2) and thereby the average edge-to-edge distance (L_{edge}) between aggregates for LMW and HMW P3EHT (Equation (3)).

$$L_{agg} = (A_{agg} / FA)^{1/2} \quad (2)$$

$$L_{edge} = L_{agg} - d_{agg} \quad (3)$$

The results, as summarized in **Table 2**, show that for HMW P3EHT percolation occurs at a higher aggregation density but a smaller aggregate size in comparison to LMW P3EHT. This suggests a higher nucleation rates and slower aggregate growths in high molecular weight films. Nevertheless L_{edge} values for the two polymers are quite close to the estimated persistence length of ≈3.0 nm for P3EHT.[36] The slightly higher L_{edge} value for HMW P3EHT here, taking to account the relatively large amounts of errors, is most likely not due to an increase in persistence length but to a higher concentration of tie-chains, which is expected for a higher molecular weight polymer. This result is in agreement with our hypothesis wherein percolation can occur when the average edge-to-edge distance between aggregates are close to the persistence length of bridging tie

Table 2. Fraction aggregates (FA), aggregate area (A_{agg}), aggregate diameter (d_{agg}), number aggregate density, distance between aggregates (L_{agg}), and edge-to-edge aggregate distance (L_{edge}) at the percolation onset for low and high molecular weight P3EHT. Average field-effect hole mobilities are also listed. For the complete time-dependent data, see supporting information.

Sample	FA	A_{agg} [nm^2]	d_{agg} [nm]	# aggregate density [nm^{-2}]	L_{agg} [nm]	L_{edge} [nm]	Average hole mobility [cm^2 V^{-1} s^{-1}]
LMW P3EHT	0.52 ± 0.02	64 ± 7	9.0 ± 0.5	0.0082 ± 0.0011	11.1 ± 0.7	2.1 ± 0.9	(3.7 ± 0.5) × 10^{-5}
HMW P3EHT	0.41 ± 0.01	43 ± 8	7.4 ± 0.7	0.0096 ± 0.0019	10.2 ± 1.0	2.8 ± 1.2	(2.0 ± 0.3) × 10^{-5}

chains. In effect, injected charges can travel efficiently within ordered domains but require bridging chains for transport between aggregates. If such aggregates are separated by a distance much greater than the persistence length of the polymer within the disordered domains, charges transported along the tie chain will likely encounter intrachain defects such as twists and torsions. These defects prevent efficient charge percolation through the film even for chains long enough to connect several aggregates. The observation of percolation onsets for low molecular weight polymer films and similar field-effect mobilities for both molecular weights further support the proposed model. We therefore conclude that efficient charge transport is achievable as long as aggregates can be bridged by polymer tie chains and are separated by a distance on the order of the chain's persistence length.

3. Conclusion

In this report we have demonstrated that P3EHT has great potential to be used as a model system for studying thin film growth and crystallization in semiconducting polymers. Through quantitative analyses of X-ray diffraction and optical techniques, we show that, in melt-recrystallized P3EHT thin films, polythiophene crystallites nucleate throughout the thickness of the film and grow anisotropically along the alkyl stacking and chain backbone directions. Nucleated crystallites are on the order of ≈3–6 nm along the chain backbone, ≈6–9 nm along the π-stacking direction and ~12 nm along the alkyl stacking direction. Aggregates grow as one-dimensional crystals only along the chain backbone direction and, as such, exhibit 1D Avrami growth. Further, nearly all films exhibit a clear percolation onset in field-effect hole mobility that corresponds to a microstructure in which the edge-to-edge distance between aggregates approaches the persistence length of the polymer. We believe such microstructures are responsible for efficient charge transport in polythiophene thin films. Although polythiophenes are generally different from new donor-acceptor type polymer semiconductors with enhanced optoelectronic properties, recent results have shown that aggregates themselves are ubiquitous and of utmost importance in dictating charge transport properties in these systems.[33]

To our knowledge these findings are the first to describe the structural mechanics and kinetics of recrystallization in semiconducting polymer thin films. Our work here provides not only a clear picture of how the nanoscale morphology of polythiophenes evolves over the crystallization process, but also direct insight into structural requirements for efficient charge transport. Specifically, we have shown that inter-aggregate distance and bridging tie chains are of great importance for charge carrier percolation in thin films. Finally the experiment results further substantiate the groundwork for future studies in polymer physics within the field. Temperature-dependent crystallization and film growth of bicomponent materials, to name a few, are currently under investigation and should lead to an even better understanding of the underlying thermodynamics of crystallization in these systems.

4. Experimental Section

Materials: Low (M_w = 6.9 kDa, M_n = 6.5 kDa, PDI = 1.06) and high (M_w = 32.8 kDa, M_n = 22.8 kDa, PDI = 1.44) molecular weight P3EHT were synthesized according to previous reports.[13] All other chemicals and solvents were purchased and used without further purifications.

Thin Film Fabrication: Films of different thicknesses are fabricated by spin casting P3EHT solutions in hot (≈80 °C) chlorobenzene with varying concentrations (5 to 40 mg mL^{-1}) at 1200–1500 rpm for 1 min. Substrates for X-ray diffraction, optical absorption, and field-effect transistor measurements are Si(100) wafers, plain glass slides, and gold-patterned, heavily doped n-type Si wafers with 200 nm of thermal oxides. All substrates were solvent cleaned and treated with UV-ozone for 20 minutes prior to spin casting. Surface treatment with hexamethyldisilazane (HMDS) and octyldecyltrichlorosilane (OTS) were performed according to our previous report.[17] Spin casting was performed in a N_2 glove box (< 10 ppm O_2) for all films. Film thicknesses are determined using a Veeco Dektak 150 profilometer.

Grazing Incidence X-Ray Diffraction: Films of different thicknesses for X-ray diffraction experiments are fabricated by spin casting P3EHT solutions in chlorobenzene with varying concentrations (5 to 40 mg mL^{-1}) onto solvent cleaned Si(100) wafers at 1200–1500 rpm for 1 min. Diffraction patterns are collected using an incident beam of 12.7 keV at a grazing angle of 0.1° and expressed as a function of the scattering vector $q = 4\pi \sin(\theta)/\lambda$. Here, θ represents half of the scattering angle, λ is the wavelength of the incident beam, q_{xy} is the component of the scattering vector parallel to the substrate plane and q_z is the component perpendicular to the substrate plane. Spin cast films are melted at 120 °C in N_2 and then quenched to room temperature. Two-dimensional diffraction patterns are collected over time after quenching (t = 0) similar to previous reports.[10]

Linear Optical Absorption: Films of different thicknesses for absorption experiments are fabricated on glass substrates under the same processing conditions as described in part A. Spectra are obtained using a Varian Cary 6000i UV-Vis-NIR spectrophotometer and fitted to a modified Frank-Spano model (see supporting information).[17,20]

Field-Effect Transistor Measurements: Thin films transistors are fabricated by spin casting P3EHT solutions onto solvent cleaned silicon substrates with a 200 nm layer of thermally grown oxide and patterned gold contacts with channel lengths between 10 to 50 μm. Transfer curves are collected under vacuum (≈10^{-3} Torr) and hole mobilities are extracted in the saturation regime (V_d = –60 V).

Supporting Information

Supporting Information is available from the Wiley Online Library or from the author.

Acknowledgements

A.S. gratefully acknowledges financial support from the National Science Foundation (DMR 1205752 award). D.T.D. is supported by a Stanford Graduate Fellowship and the National Science Foundation Graduate Research Fellowship. S.M. is supported by a Stanford Graduate Fellowship. J.D. was supported by the Center for Advanced Molecular Photovoltaics (Award No. KUS-C1-015-21), made by King Abdullah University of Science and Technology (KAUST). A portion of this research was carried out at the Stanford Synchrotron Radiation Lightsource, a national user facility operated by Stanford University on behalf of the U.S. Department of Energy, Office of Basic Energy Sciences.

Received: December 20, 2013
Revised: February 13, 2014
Published online: April 9, 2014

[1] C. J. Brabec, S. Gowrisanker, J. J. M. Halls, D. Laird, S. Jia, S. P. Williams, *Adv. Mater.* **2010**, *22*, 3839.
[2] P. M. Beaujuge, J. M. J. Fréchet, *J. Am. Chem. Soc.* **2011**, *133*, 20009.
[3] A. Facchetti, *Chem. Mater.* **2011**, *23*, 733.
[4] H. Minemawari, T. Yamada, H. Matsui, J. Tsutsumi, S. Haas, R. Chiba, R. Kumai, T. Hasegawa, *Nature* **2011**, *475*, 364.
[5] G. Li, R. Zhu, Y. Yang, *Nat. Photonics* **2012**, *6*, 153.
[6] K. Vandewal, S. Himmelberger, A. Salleo, *Macromolecules* **2013**.
[7] J. Rivnay, S. C. B. Mannsfeld, C. E. Miller, A. Salleo, M. F. Toney, *Chem. Rev.* **2012**, *112*, 5488.
[8] A. Salleo, *Mater. Today* **2007**, *10*, 38.
[9] J. Rivnay, S. C. B. Mannsfeld, C. E. Miller, A. Salleo, M. F. Toney, *Chem. Rev.* **2012**, *112*, 5488.
[10] B. W. Boudouris, V. Ho, L. H. Jimison, M. F. Toney, A. Salleo, R. a. Segalman, *Macromolecules* **2011**, *44*, 6653.
[11] K. Vakhshouri, E. D. Gomez, *Macromol. Rapid Commun.* **2012**, 2133.
[12] K. W. Chou, B. Yan, R. Li, E. Q. Li, K. Zhao, D. H. Anjum, S. Alvarez, R. Gassaway, A. Biocca, S. T. Thoroddsen, A. Hexemer, A. Amassian, *Adv. Mater.* **2013**, *25*, 1923.
[13] V. Ho, B. W. Boudouris, R. a. Segalman, *Macromolecules* **2010**, *43*, 7895.
[14] M. Brinkmann, P. Rannou, *Macromolecules* **2009**, *42*, 1125.
[15] Y.-K. Lan, C.-I. Huang, *J. Phys. Chem. B* **2009**, *113*, 14555.
[16] S. C. B. Mannsfeld, M. L. Tang, Z. Bao, *Adv. Mater.* **2011**, *23*, 127.
[17] D. Duong, M. Toney, A. Salleo, *Phys. Rev. B* **2012**, *86*, 205205.
[18] F. C. Spano, *J. Chem. Phys.* **2005**, *122*, 234701.
[19] J. Clark, J.-F. Chang, F. C. Spano, R. H. Friend, C. Silva, *Appl. Phys. Lett.* **2009**, *94*, 163306.
[20] S. T. Turner, P. Pingel, R. Steyrleuthner, E. J. W. Crossland, S. Ludwigs, D. Neher, *Adv. Funct. Mater.* **2011**, *21*, 4640.
[21] D. T. Duong et al., *unpublished*.
[22] L. H. Jimison, S. Himmelberger, D. T. Duong, J. Rivnay, M. F. Toney, A. Salleo, *J. Polym. Sci. Part B Polym. Phys.* **2013**, *51*, 611.
[23] J. Gierschner, Y.-S. Huang, B. Van Averbeke, J. Cornil, R. H. Friend, D. Beljonne, *J. Chem. Phys.* **2009**, *130*, 044105.
[24] A. K. Jena, C. Chaturvedi, *Phase transformation in materials*, Prentice Hall, **1992**.
[25] D. M. DeLongchamp, R. J. Kline, E. K. Lin, D. a. Fischer, L. J. Richter, L. a. Lucas, M. Heeney, I. McCulloch, J. E. Northrup, *Adv. Mater.* **2007**, *19*, 833.
[26] S. Pal, A. K. Nandi, *J. Appl. Polym. Sci.* **2006**, *101*, 3811.
[27] S. Malik, A. K. Nandi, *J. Polym. Sci. Part B Polym. Phys.* **2002**, *40*, 2073.
[28] S. Pal, A. K. Nandi, *Polymer* **2005**, *46*, 8321.
[29] W.-R. Wu, U.-S. Jeng, C.-J. Su, K.-H. Wei, M.-S. Su, M.-Y. Chiu, C.-Y. Chen, W.-B. Su, C.-H. Su, A.-C. Su, *ACS Nano* **2011**, *5*, 6233.
[30] F. Dinelli, M. Murgia, P. Levy, M. Cavallini, F. Biscarini, *Phys. Rev. Lett.* **2004**, *92*, 90.
[31] J.-F. Chang, J. Clark, N. Zhao, H. Sirringhaus, D. Breiby, J. Andreasen, M. Nielsen, M. Giles, M. Heeney, I. McCulloch, *Phys. Rev. B* **2006**, *74*, 115318.
[32] O. G. Reid, J. a. N. Malik, G. Latini, S. Dayal, N. Kopidakis, C. Silva, N. Stingelin, G. Rumbles, *J. Polym. Sci. Part B Polym. Phys.* **2012**, *50*, 27.
[33] R. Noriega, J. Rivnay, K. Vandewal, F. P. V Koch, N. Stingelin, P. Smith, M. F. Toney, A. Salleo, *Nat. Mater.* **2013**, *12*, 1.
[34] G. W. Heffner, D. S. Pearson, *Macromolecules* **1991**, *24*, 6295.
[35] R. J. Kline, M. D. Mcgehee, E. N. Kadnikova, J. Liu, J. M. J. Frechet, M. F. Toney, *Macromolecules* **2005**, *38*, 3312.
[36] B. McCulloch, V. Ho, M. Hoarfrost, C. Stanley, C. Do, W. T. Heller, R. A. Segalman, *Macromolecules* **2013**, *46*, 1899.